Applied Mathematical Modelling 76 (2019) 607–616

Contents lists available at ScienceDirect

Applied Mathematical Modelling

journal homepage: www.elsevier.com/locate/apm

Theoretical model for swirling thin film flows inside nozzles with converging-diverging shapes

Boo-Hyoung Bang[a,b], Yong-Il Kim[a], Seokgyu Jeong[c], Youngbin Yoon[c], Alexander L. Yarin[d,*], Sam S. Yoon[a,*]

[a] School of Mechanical Engineering, Korea University, Seoul 136-713, Republic of Korea
[b] Technology Development Team, Daewoo Institute of Construction Technology, 60, Songjuk-dong, Jangan-gu 440-210, Suwon, Republic of Korea
[c] Department of Mechanical and Aerospace Engineering, Seoul National University, Seoul 08826, Republic of Korea
[d] Department of Mechanical and Industrial Engineering, University of Illinois at Chicago, 842 W. Taylor St., Chicago, IL 60607-7022, USA

ARTICLE INFO

Article history:
Received 13 February 2019
Revised 4 June 2019
Accepted 17 June 2019
Available online 22 June 2019

Keywords:
Swirl jet
Thin film
Nozzle geometry
Analytical solution
Swirl strength
Reynolds

ABSTRACT

A quasi-one-dimensional model was developed to describe a swirling, thin, liquid film inside nozzles with different wall profiles. The model quantifies the effects of swirl strength, initial film thickness, and Reynolds and Weber numbers on the film thickness along the nozzle surface. Moreover, the model allows for a rapid (at least, qualitative) evaluation of different effects, e.g. of the swirl strength and nozzle geometry, and can serve as a benchmark case for the subsequent more involved numerical simulations. Steady-state solutions are presented as a function of various parameters. The effect of the nozzle geometry on film thickness is explored. As swirling flow entered the expanding (diverging) section of the nozzle, film thickness decreased to satisfy continuity (to conserve mass). Conversely, film thickness increased upon entering the contracting (converging) region of the nozzle. Geometric effects controlled film thicknesses much more than other flow parameters. This quasi-one-dimensional model for a swirling thin film can be useful for designing a swirl jet used in various industrial applications.

1. Introduction

Pressure-swirl atomizers have been widely used in liquid-rocket, gas-turbine, and internal-combustions engines, painting, air-conditioning, and fire suppression because they are easy to manufacture and yield high-quality atomization at a low cost [1–6]. In combustion applications, spray-atomizer characteristics affect combustion stability and vice versa [7,8]. Operating conditions that determine the Reynolds, Weber, Ohnesorge, and Rossby numbers, as well as nozzle geometries and ambient conditions, affect the overall performance of pressure-swirl atomizers. Pressure-swirl atomizers must be characterized to enable an optimization of the spray design that facilitates stable combustion.

Recently, a review paper summarized experimental, theoretical, and numerical studies on pressure-swirl atomizers [9]. Numerical studies of flows in swirl atomizers are available [1,5,10–14]. Relevant theoretical studies date back to the work of Taylor [15,16] and Binnie and Harris [17] who solved the continuity and momentum equations for swirling flow within a cylinder. Chinn [18,19] revisited the theories of Taylor and Binnie and Harris and further elucidated the details of their

* Corresponding authors.
E-mail addresses: ayarin@uic.edu, skyoon@korea.ac.kr (S.S. Yoon).

https://doi.org/10.1016/j.apm.2019.06.025
0307-904X/

derivation. More recently, Amini [1] applied the theory of Binnie and Harris [17] to a more complex nozzle that included an upper swirling chamber, a middle converging chamber, and a constant-diameter exit orifice. However, these theoretical approaches characterizing internal swirling jets are limited within the scope of the works of [15] and [17]. Nevertheless, these theoretical models are quite useful for providing boundary conditions at the nozzle exit, so that the issuing flow can be simulated with proper initial conditions. Consideration of various internal geometries of a swirl atomizer based on a relatively simple tool is thus valuable. Operating conditions such as inertia, swirl strength, and fluid surface tension could also be considered in the model. To the best of our knowledge, this demand has not yet been satisfied.

This manuscript outlines a novel quasi-one-dimensional approach that characterizes thin, swirling, liquid-film flows along the internal wall of a nozzle of an arbitrary shape. This new theoretical/numerical approach employs the continuity and momentum balance equations in the quasi-one-dimensional approximation of [20], which reduces the 3D fluid mechanics equations using an analog of the Karman–Pohlhausen method. These governing equations in principle allow for a straightforward description of swirling thin films flowing inside an axisymmetric nozzle with arbitrary walls accounting for the inertia, swirl, surface tension, and the gas pressure fluctuations in the cavity. Note also, that the novel quasi-one-dimensional approach for the film flows in converging-diverging nozzles developed here is related to those used in the theory of free liquid jets and films [20], rather than to the preceding literature on nozzle flows.

2. Modeling description

2.1. Physical estimates

In journal-bearing literature [21], the critical Reynolds number (Re_c=2000–5000) corresponding to the laminar-to-turbulent transition is based on the largest velocity in the liquid film and the gap width. For radial free films on a disk, [22–25] theoretically predicted the laminar-to-turbulent transition at Re_c=450, while [26] measured Re_c=470. In the experiments of [27], water was used as the working fluid with a mass flow rate of $\dot{M}$=57 g/s, nozzle exit diameter of D_0=0.6 cm, exit velocity of V_0=1.24 × 10^3 cm/s, and water density of ρ=1 g/cm^3 and kinematic viscosity ν=0.01 cm/s. Then, the film thickness at the exit is: [27]

$$h_0 = \frac{\dot{M}}{\rho \pi D_0 V_0} = 0.024\ cm \tag{1}$$

Accordingly, the Reynolds number at the exit conditions is:

$$Re_{exit} = \frac{V_0 h_0}{\nu} = 2976 \tag{2}$$

which is marginally higher than Re_c for the comparable flows mentioned above. Thus, film flow cannot be a fully developed turbulent flow. Rather, it is intermittent; presumably resembling a laminar velocity profile with occasional perturbation waves.

The values of the critical Reynolds number for the laminar-turbulent transition in the film flows can vary depending on the particular geometry, and two different values are mentioned above: Re_c=470 and 2000. Note that according to [21] Re_c can be as high as 5000 (which is now mentioned in the revised version). That means that irrespective of a particular geometry, the critical Reynolds number is of the order of 10^3 to 10^4. The estimate (2) shows that in the present case the turbulence effects are probably negligibly small, and the film flow can be treated as laminar.

2.2. The governing equations

An axially symmetric film flows inside an axially symmetric nozzle is sketched in Fig. 1. The nozzle has an arbitrary periodically converging-diverging profile. The film can swirl about the nozzle axis, with all the flow components (the swirling and longitudinal) being axisymmetric, as well as an axisymmetric gas flow through the nozzle being also possible. Gas pressure is assumed to depend on the axial location, x, and time, t, i.e., $p_{gas}(x, t)$ is known.

The longwave approximation is assumed, i.e., film thickness, h, is assumed to be much smaller than the characteristic longitudinal scale, L (cf. Fig. 1), which allows one to recourse to the quasi-one-dimensional approximation. The nozzle shape is specified as $R(x)$.

In the quasi-one-dimensional approximation, the continuity equation expressing the mass balance for the film is [20]:

$$\frac{\partial h}{\partial t} + \frac{1}{R\lambda}\frac{\partial R h \bar{v}_s}{\partial x} = 0 \tag{3}$$

where $h(x, t)$ is the film thickness, $\bar{v}_s(x, t)$ is the average cross-sectional longitudinal velocity in the film reckoned along the nozzle generatrix, and the generatix "stretching ratio" is related to the nozzle radius as:

$$\lambda = \sqrt{1 + \left(\frac{dR}{dx}\right)^2}, \tag{4}$$

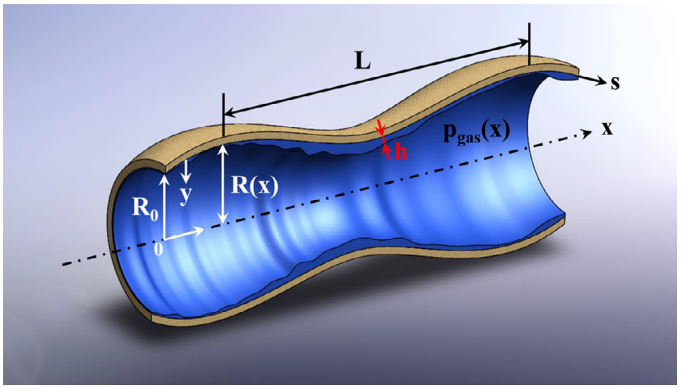

Fig. 1. Sketch of a film flowing inside a periodically converging-diverging nozzle.

Here, the analog of the Karman–Pohlhausen method is used [28–30] with the longitudinal and swirling velocity profiles being assumed locally parabolic:

$$v_s = A(x,t)y + B(x,t)y^2$$
$$v_\theta = C(x,t)y + D(x,t)y^2 \tag{5}$$

where y is the coordinate reckoned normally inward from the inner nozzle wall, and functions A, B, C, and D are described below.

The preceding velocity profiles (5) satisfy the no-slip conditions at the nozzle wall, $y=0$, where both v_s and v_θ vanish. The tractions imposed at the film surface by the gas are typically negligibly small compared to the internal stresses in the liquid, because the liquid viscosity is at least two orders of magnitude higher than that of the gas. Accordingly, the shear stresses at the film surface should vanish:

$$\left.\frac{\partial v_s}{\partial y}\right|_{y=h} = 0, \quad \left.\frac{\partial v_\theta}{\partial y}\right|_{y=h} = 0 \tag{6}$$

Together, Eqs. (5) and (6) yield $B=-½A/h$ and $D=-½C/h$, and thus:

$$v_s = A(x,t)\left(y - \frac{y^2}{2h}\right), \quad v_\theta = C(x,t)\left(y - \frac{y^2}{2h}\right) \tag{7}$$

From the preceding equations:

$$\bar{v}_s(x,t) = \frac{1}{h}\int_0^h v_s dy = \frac{A(x,t)h}{3}. \tag{8}$$

Thus, Eqs. (3) and (8) yield the continuity equation as:

$$\frac{\partial h}{\partial t} + \frac{1}{3R\lambda}\frac{\partial A h^2 R}{\partial x} = 0 \tag{9}$$

Note that the axially symmetric continuity equation in cylindrical coordinates is [29]:

$$\frac{\partial r v_r}{\partial r} + \frac{\partial r v_x}{\partial x} = 0 \tag{10}$$

where r is the radial coordinate, and v_r and v_x are the radial and axial velocity components, respectively.

Because in the quasi-one-dimensional approximation the nozzle radius varies gradually, $v_x \approx v_s$, $\partial/\partial r \approx -\partial/\partial y$, and $r \approx R$ in the film, and integrating Eq. (10) yields:

$$v_r \approx \int_0^y \frac{\partial v_s}{\partial x} dy \tag{11}$$

This equation, combined with the first Eq. (7) and accounting for the fact that in a thin film $h \sim y$, yields:

$$v_r \approx \frac{y^2}{3}\frac{\partial A}{\partial x} \tag{12}$$

It should be emphasized that in the longwave quasi-one-dimensional approximation used here, the term which involves multiplication of two derivatives in x, e.g., $(\partial A/\partial x)(\partial h/\partial x)$ is negligibly small compared to the terms which were retained.

Consider now the radial projection of the Navier–Stokes equation in cylindrical coordinates [29]. For strongly swirling flows in the film, the leading-order effect is due to the centrifugal acceleration. Hence, the radial projection of the Navier–Stokes equation reduces to:

$$\frac{\partial p}{\partial r} = \frac{\rho v_\theta^2}{r} \tag{13}$$

where p is the pressure in the liquid film.

In the quasi-one-dimensional approximation in a thin liquid film, $\partial/\partial r \approx -\partial/\partial y$ and $r \approx R$, which transforms Eq. (13) into:

$$\frac{\partial p}{\partial y} = -\frac{\rho v_\theta^2}{R} \tag{14}$$

Integrating this equation and applying the boundary condition for the pressure at the film surface that includes capillary pressure, yields:

$$p = -\frac{\rho}{R}\int_h^y v_\theta^2 dy + p_{gas}(x,t) - \frac{\sigma}{\lambda}\frac{\partial}{\partial x}\left(\frac{1}{\lambda}\frac{\partial h}{\partial x}\right) \tag{15}$$

where σ is the surface tension.

Assuming constant pressure across the film in the first approximation, it yields in the average:

$$\overline{p} = \frac{\rho}{R}\int_0^h v_\theta^2 dy + p_{gas}(x,t) - \frac{\sigma}{\lambda}\frac{\partial}{\partial x}\left(\frac{1}{\lambda}\frac{\partial h}{\partial x}\right) \tag{16}$$

Substituting the second Eq. (7) into Eq. (16) and evaluating the integral over y, one obtains results in:

$$\bar{p} = \frac{2}{15}\frac{\rho h^3 C^2}{R} + p_{gas}(x,t) - \frac{\sigma}{\lambda}\frac{\partial}{\partial x}\left(\frac{1}{\lambda}\frac{\partial h}{\partial x}\right) \tag{17}$$

Consider now the azimuthal projection of the Navier–Stokes equation in cylindrical coordinates [29]. In the quasi-one-dimensional approximation in a thin liquid film in the light of Eq. (12), the leading terms of this equation reduce to:

$$\rho\frac{\partial v_\theta}{\partial t} = \mu\frac{\partial^2 v_\theta}{\partial y^2} \tag{18}$$

where μ is the liquid viscosity.

Substituting the second Eq. (7) into Eq. (18) and integrating across the film yields the following equation for the "swirling" function, C:

$$\frac{\partial C}{\partial t} = -\nu\frac{3C}{h^2} \tag{19}$$

Similarly, the longitudinal projection of the Navier–Stokes equation in cylindrical coordinates [29] in the quasi-one-dimensional approximation for a thin liquid film, accounting for Eq. (12), yields:

$$\rho\frac{\partial v_s}{\partial t} = -\frac{\partial \bar{p}}{\partial x} + \mu\frac{\partial^2 v_s}{\partial y^2} \tag{20}$$

Substituting the first Eq. (7) into Eq. (20) and integrating across the film yields the following equation for the "longitudinal" function, A:

$$\frac{\partial A}{\partial t} = -\frac{3}{\rho h}\frac{\partial \bar{p}}{\partial x} - \nu\frac{3A}{h^2} \tag{21}$$

Combining Eqs. (9), (17), (19) and (21) results in a system of three partial differential equations describing the interrelationship between $h(x, t)$, $C(x, t)$ and $A(x, t)$:

$$\frac{\partial h}{\partial t} + \frac{1}{3R\lambda}\frac{\partial A h^2 R}{\partial x} = 0,$$
$$\lambda = \sqrt{1 + \left(\frac{dR}{dx}\right)^2}, \tag{22}$$

$$\frac{\partial C}{\partial t} = -\nu\frac{3C}{h^2} \tag{23}$$

$$\frac{\partial A}{\partial t} = -\frac{3}{\rho h}\frac{\partial}{\partial x}\left[\frac{2}{15}\frac{\rho h^3 C^2}{R} + p_{gas}(x,t) - \frac{\sigma}{\lambda}\frac{\partial}{\partial x}\left(\frac{1}{\lambda}\frac{\partial h}{\partial x}\right)\right] - \nu\frac{3A}{h^2} \tag{24}$$

The initial and boundary conditions are:

$$\begin{aligned} h(x,0) &= h_0, \\ C(x,0) &= C_0, \\ A(x,0) &= A_0, \end{aligned} \tag{25}$$

and

$$\begin{aligned} h(0,t) &= h^0(t)\,, \\ C(0,t) &= C_0, \\ A(0,t) &= A_0, \end{aligned} \tag{26}$$

where the nozzle entrance is $x=0$. Also, h_0, C_0 and A_0 are constants, and $h^0(t)$ describes perturbations in the film thickness at the nozzle entrance.

The thin-film volumetric flow rate at the nozzle entrance is:

$$Q(t) = \left.\frac{2\pi}{3} R\lambda A h^2\right|_{x=0} \tag{27}$$

The parameters in the governing equations are rendered dimensionless using the following scales: A_0^{-1} for t, h_0 for h, A_0 for A and C, the entrance radius of the nozzle R_0 for R and x, $\rho h_0 R_0 A_0^2$ for p_{gas}, and $R_0 h_0^2 A_0$ for Q. Then, Eqs. (22)–(27) take the following dimensionless form (where overbars are omitted for brevity):

$$\begin{aligned} &\frac{\partial h}{\partial t} + \frac{H_0}{3R\lambda}\frac{\partial A h^2 R}{\partial x} = 0, \\ &\lambda = \sqrt{1+\left(\frac{dR}{dx}\right)^2}, \end{aligned} \tag{28}$$

$$\frac{\partial C}{\partial t} = -\frac{3}{Re}\frac{C}{h^2} \tag{29}$$

$$\frac{\partial A}{\partial t} = -\frac{3}{h}\frac{\partial}{\partial x}\left[H_0^2\frac{2}{15}\frac{h^3C^2}{R} + p_{gas}(x,t) - \frac{1}{We}\frac{1}{\lambda}\frac{\partial}{\partial x}\left(\frac{1}{\lambda}\frac{\partial h}{\partial x}\right)\right] - \frac{3}{Re}\frac{A}{h^2} \tag{30}$$

$$\begin{aligned} h(x,0) &= 1, \\ C(x,0) &= M_0, \\ A(x,0) &= 1, \end{aligned} \tag{31}$$

$$\begin{aligned} h(0,t) &= H^0(t), \\ C(0,t) &= M_0, \\ A(0,t) &= 1, \end{aligned} \tag{32}$$

$$Q(t) = \left.\frac{2\pi}{3}\left[H^0(t)\right]^2\lambda\right|_{x=0} \tag{33}$$

The dimensionless groups in Eqs. (28)–(33) read:

$$H_0 = \frac{h_0}{R_0}, \quad Re = \frac{h_0^2 A_0}{\nu}, \quad We = \frac{\rho R_0^3 A_0^2}{\sigma}, \quad M_0 = \frac{C_0}{A_0} \tag{34}$$

where Re and We denote the Reynolds and the Weber numbers, respectively, and all the parameters can be independently varied, in principle, in experiments.

The dimensionless function $H^0(t)=h_0(t)/h_0$ can be, for example:

$$H^0(t) = 1 + 0.1\sin(\omega t), \tag{35}$$

where frequency ω is rendered dimensionless by A_0.

Eqs. (28)–(30) require only the upstream boundary conditions and can be integrated using an appropriate marching numerical method. They were numerically integrated subject to the initial conditions (31) and the boundary conditions (32) and (35). The integration interval in x was $0 \le x \le \Lambda$, where the nozzle length Λ was rendered dimensionless by R_0, i.e. $\Lambda = L/R_0$.

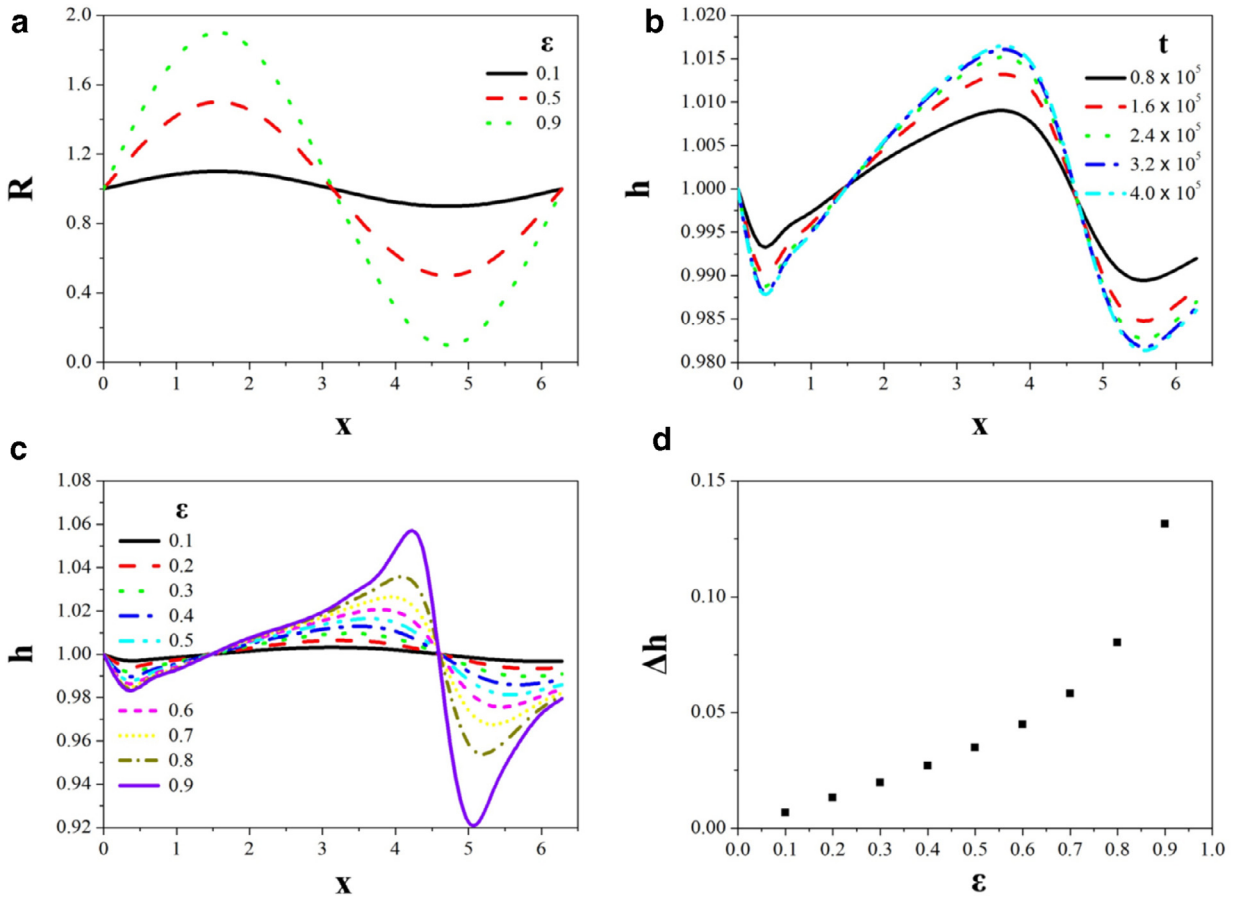

Fig. 2. Film thickness, h, variation in the axial direction, x, for nozzle geometries with dimensionless amplitude, ε, from 0.1 to 0.9. Here, H_0=0.0001 and Re=3000. (a) The nozzle profiles for ε=0.1, 0.5, and 0.9. (b) The temporal evolution of the solutions for ε=0.5 with the steady state being achieved by $t=4\times10^5$. (c) Steady-state solutions for $0.1\leq\varepsilon\leq0.9$. (d) Film-thickness change, $\Delta h=h_{\max}-h_{\min}$ as a function of ε. The calculations were conducted with $H^0(t)\equiv1$, which guarantees that a steady-state exists.

3. Results and discussion

Assume a periodically converging-diverging nozzle profile as:

$$R(x)=R_0(1+\varepsilon\sin x) \tag{36}$$

where x was rendered dimensionless by R_0 and ε is a dimensionless amplitude.

Assuming negligible gas compressibility throughout the nozzle, Bernoulli's equation relates gas pressures and velocities:

$$p_{gas}(x)=p_0+\frac{\rho_{gas}V_{0,gas}^2}{2}-\frac{\rho_{gas}V_{gas}^2(x)}{2} \tag{37}$$

where p_0 is the gas pressure at the nozzle entrance, ρ_{gas} is the gas density, and $V_{0,\text{gas}}$ is the gas velocity at the nozzle entrance.

Assuming a constant volumetric gas flow rate, Q_{gas}, the mass balance specifies the gas flow velocity as:

$$V_{0,gas}=\frac{Q_{gas}}{\pi R_0^2},$$
$$V_{gas}=\frac{Q_{gas}}{\pi R_0^2[1+\varepsilon\sin(x)]^2}. \tag{38}$$

Substituting Eqs. (38) into Eq. (37), one obtains the dimensionless gas pressure in the following form:

$$p_{gas}(x)=P+W\left\{1-\frac{1}{[1+\varepsilon\sin(x)]^4}\right\} \tag{39}$$

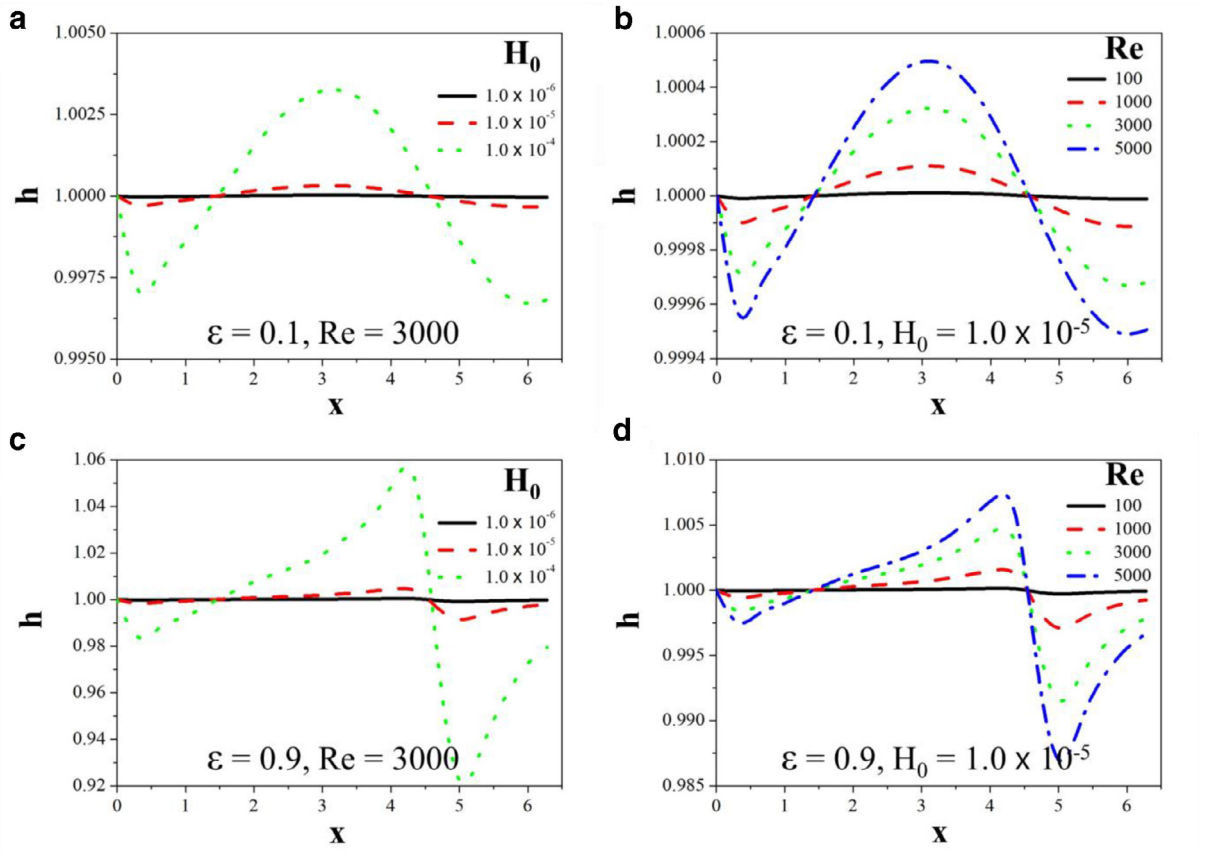

Fig. 3. Liquid film thickness distributions for various H_0 and *Re*. (a) The effect of H_0 on h at ε=0.1 and *Re*=3000. (b) The effect of *Re* on h at ε=0.1 and H_0=10^{-5}. (c) The effect of H_0 on h at ε=0.9 and *Re*=3000. (d) The effect of *Re* on h at ε=0.9 and H_0=10^{-5}. The calculations were conducted with $H^0(t) \equiv 1$, which guarantees that a steady-state exists.

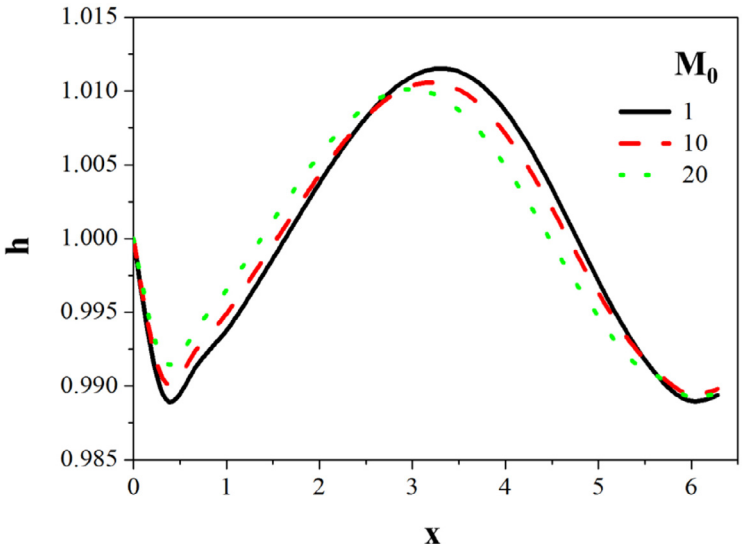

Fig. 4. Longitudinal distribution of the film thickness h for various swirl strengths, M_0, for ε=0.1, H_0=0.01, and *Re*=100. The calculations were conducted with $H^0(t) \equiv 1$, which guarantees that a steady-state exists.

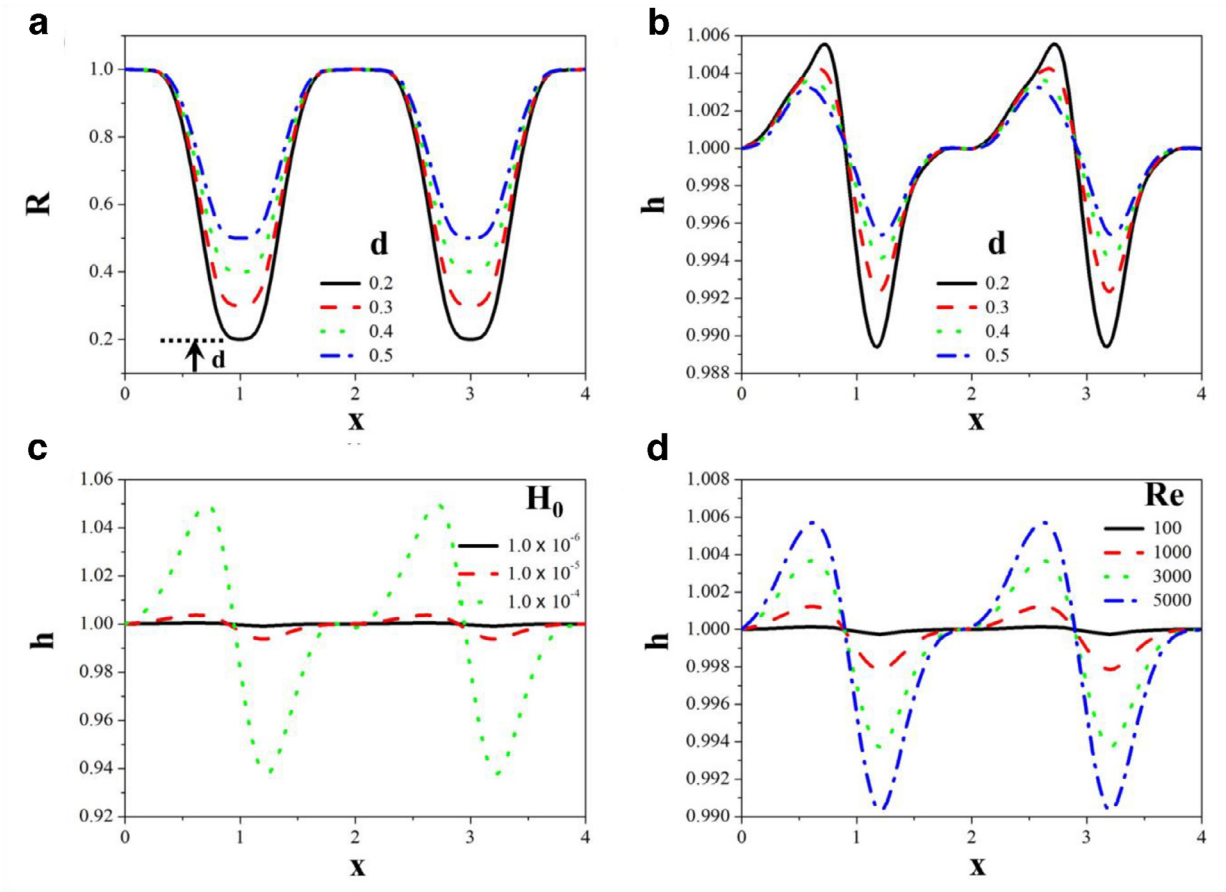

Fig. 5. (a) The non-sinusoidal nozzle geometry with various throat curvatures determined by d from the $0.2 \le d \le 0.5$ range. (b) The film thickness distribution h for different d at $H_0 = 1.0 \times 10^{-5}$ and $Re = 3000$. (c) The effect of H_0 on h at $d = 0.3$ and $Re = 3000$. (d) The effect of Re on h at $d = 0.3$ and $H_0 = 1.0 \times 10^{-5}$.

with the additional dimensionless groups being:

$$P = \frac{p_0}{\rho h_0 R_0 A_0^2}, \quad W = \frac{\rho_{gas} Q_{gas}^2}{2\left(\pi R_0^2\right)^2 \rho h_0 R_0 A_0^2} \tag{40}$$

It should be emphasized that the additional normal stresses acting on the film from the gas flow are of the order of $\rho_{gas} V_{gas}^2$, whereas the shear tractions imposed of the film by the gas flow are of the order of $\mu_{gas} V_{gas}/h$, where μ_{gas} is the gas viscosity, The ratio of the former to the latter is of the order of $Re_{gas} = \rho_{gas} V_{gas} h/\mu_{gas}$. Taking for the estimate air as the gas, $V_{gas} \sim 10\, m/s$ and $h \sim 1\, mm$, one obtains $\mathrm{Re}_{gas} \sim 10^3$, which shows that the viscous tractions of air are negligibly small compared to the additional normal stresses. Moreover, the results discussed below show that even the latter are immaterial in the present case compared to the other effects.

Fig. 2(a) shows the nozzle profiles corresponding to Eq. (36) for ε=0.1, 0.5, and 0.9. The nozzle length is 2π to comprise a full sine period. The nozzle diverges at $0 < x < \pi/2$, converges at $\pi/2 < x < 3\pi/2$, and then diverges again up to the exit location at $x = 2\pi$. The initial dimensionless film thickness was taken as H_0=0.0001, resulting in an extremely thin swirling film. Fig. 2(b) shows the temporal evolution of the dimensionless film thickness over the entire nozzle under consideration. The film thickness decreased slightly at the beginning of the nozzle ($0 < x < 0.4$). Then the film thickness increased downstream up to $x = 3.6$ in the converging section, and then decreased and increased again from about $x = 5.5$. The steady-state film thickness was achieved by $t = 4.0 \times 10^5$. Fig. 2(c) illustrates how steady-state distributions of the film thickness h vary with ε along the nozzle. It is interesting to note that the film thickness variation is not entirely concerted with the nozzle profile variation. For example, the film thickness begins to decrease from about $x = 3.6 - 4$ still in the converging part of the nozzle. Fig. 2(d) summarizes changes in h ($\Delta h = h_{\max} - h_{\min}$) with ε. An increase in the amplitude of the nozzle profile variation magnifies the film thickness variation, albeit the latter was never more than 15% of h_0.

Fig. 3(a) and (b) illustrates how the film thickness varies along the nozzle at different values of H_0 and Re, respectively, at ε=0.1. The observed trends are similar to those in Fig. 2, but the longitudinal variation in h is magnified as the values of

H_0 and Re increased. A minimal longitudinal variation in h was observed for $H_0<10^{-5}$ and $Re<1000$. When the amplitude of the nozzle profile variation increased to $\varepsilon=0.9$ as in Fig. 3(c) and (d), the longitudinal variation of h also increased. The effect of the Weber number appeared to be negligible in the $10^3<We<10^7$ range (the corresponding results are not shown here). The predicted minimal influence of the surface tension is consistent with the findings of [17].

Fig. 4 depicts the predicted longitudinal distribution of the film thickness h for several swirl strengths, $M_0=C_0/A_0$ ($M_0=0$ would correspond to the absence of swirl, and the increasing values of M_0 correspond to the increasing swirl). Changing M_0 at $Re>500$ had minor effect on h. However, for $Re=100$ and the initially thick film at the nozzle entrance, $H_0=0.01$, increasing M_0 slightly decreased the longitudinal variation in h and slightly shifted the positions of the minima and maximum.

Fig. 5(a) demonstrates the nozzle shapes for different curvatures, with $d = 0.2$, 0.3, 0.4 and 0.5. This nozzle shape is not defined by a sinusoidal wave of Eq. (36), but rather is comprised of a flat surface on top and deep 'valleys' toward the centerline of the nozzle. The throat of the nozzle is formed near the centerline from which the dimensionless d is reckoned, as indicated in Fig. 5(a). This nozzle is periodic in shape with the dimensional period of $\Delta x = 2$, with two periods being simulated up to $x_{\max}=4$. Fig. 5(b) illustrates the effect of d on the film thickness, h. The thickness increases and decreases when the nozzle converges and diverges, respectively, at $H_0=1.0\times10^{-5}$ and $Re=3000$, but the thickness variation is not entirely concerted with the nozzle profile, as in Fig. 2. Fig. 5(c) and (d) shows the effect of H_0 and Re on h, respectively. When the value of H_0 and Re increases, the film thickness variation along the nozzle is magnified.

4. Conclusion

The quasi-one-dimensional approximation based on the Karman–Pohlhausen method was used to obtain the simplified continuity and momentum balance equations. These equations were used to model swirling thin film flows within a converging-diverging nozzle. It was shown that the steady-state longitudinal variation of the film thickness h along the nozzle is not entirely concerted with the converging-diverging nozzle profile. Also, as the amplitude of the nozzle profile variation was increased, the longitudinal variation in the steady-state film thickness also increased. An increase in the ratio of the entrance film thickness to the nozzle radius and in the Reynolds number had a similar effect on h. On the other hand, the swirling strength had a relatively minor effect on h, albeit at the lower Reynolds number of 100, the longitudinal distribution of the film thickness was deformed at an increased swirl strength. The effect of the Weber number was negligible in the $10^3<We<10^7$ range. It should be emphasized that the quasi-one-dimensional approximation is valid for thin liquid films and slowly varying nozzle radius, which at least, prevents flow separation. Nozzles with abrupt change in the generatrix and thick film flows require another approach. This work is underway, and will be presented in the subsequent publication.

Acknowledgment

This research was supported by the Technology Development Program to Solve Climate Changes of the National Research Foundation (NRF) funded by the Ministry of Science, ICT & Future Planning (NRF-2016M1A2A2936760). This work was supported by the National Research Council of Science & Technology (NST) grant by the Korea government (MSIP) (No. CRC-16-02-KICT), NRF-2017R1A2B4005639, and NRF-2013R1A5A1073861.

References

[1] G. Amini, Liquid flow in a simplex swirl nozzle, Int. J. Multiph. Flow 79 (2016) 225–235.
[2] T. Li, K. Nishida, H. Hiroyasu, Droplet size distribution and evaporation characteristics of fuel spray by a swirl type atomizer, Fuel 90 (2011) 2367–2376.
[3] J. Liu, X.-Q. Zhang, Q.-L. Li, Z.-G. Wang, Effect of geometric parameters on the spray cone angle in the pressure swirl injector, Proc. Inst. Mech. Eng. Part G: J. Aerosp. Eng. 227 (2013) 342–353.
[4] H. Ma, X. Wu, F. Feng, D. Wang, C. Yang, C. Zhuo, An experimental study on fuel spray-induced vortex-like structures, Exp. Therm. Fluid Sci. 57 (2014) 335–343.
[5] J. Xue, M. Jog, S. Jeng, E. Steinthorsson, M. Benjamin, Effect of geometric parameters on simplex atomizer performance, AIAA J. 42 (2004) 2408–2415.
[6] S. Yao, J. Zhang, T. Fang, Effect of viscosities on structure and instability of sprays from a swirl atomizer, Exp. Therm. Fluid Sci. 39 (2012) 158–166.
[7] V. Bazarov, Influence of propellant injector stationary and dynamic parameters on high frequency combustion stability, in: Proceedings of the Thirty-Second AIAA, ASME, SAE, and ASEE, Joint Propulsion Conference and Exhibit, AIAA Paper, 1996, p. 3119.
[8] R. Kesselring, R. Nelson, K. Sprouse, Engine hydraulic stability, Final Report, NASA CR-151499, (1977).
[9] G.A. Vijay, N.S.V. Moorthi, A. Manivannan, Internal and external flow characteristics of swirl atomizers: a review, Atom. Sprays 25 (2015) 153–188.
[10] S.K. Dash, M.R. Halder, M. Peric, S.K. Som, Formation of air core in nozzles with tangential entry, J. Fluids Eng. 123 (2001) 829–835.
[11] A.A. Ibrahim, M.A. Jog, Nonlinear breakup model for a liquid sheet emanating from a pressure-swirl atomizer, J. Eng. Gas Turb. Power 129 (2007) 945–953.
[12] Y. Liao, A.T. Sakman, S.M. Jeng, M.A. Jog, M.A. Benjamin, A comprehensive model to predict simplex atomizer performance, J. Eng. Gas Turb. Power 121 (1999) 285–294.
[13] A. Mandal, M.A. Jog, J. Xue, A.A. Ibrahim, Flow of power-law fluids in simplex atomizers, Int. J. Heat Fluid Flow 29 (2008) 1494–1503.
[14] A. Nouri-Borujerdi, A. Kebriaee, Numerical simulation of laminar and turbulent two-phase flow in pressure-swirl atomizers, AIAA J. 50 (2012) 2091–2101.
[15] G. Taylor, The mechanics of swirl atomizers, in: Proceedings of the Seventh International Congress of Applied Mechanics, 1948, pp. 280–285.
[16] G. Taylor, The boundary layer in the converging nozzle of a swirl atomizer, Q. J. Mech. Appl. Math. 3 (1950) 129–139.
[17] A. Binnie, D. Harris, The application of boundary-layer theory to swirling liquid flow through a nozzle, Q. J. Mech. Appl. Math. 3 (1950) 89–106.
[18] J.J. Chinn, An appraisal of swirl atomizer inviscid flow analysis, part 1: the principle of maximum flow for a swirl atomizer and its use in the exposition and comparison of early flow analyses, Atom. Sprays 19 (2009) 263–282.
[19] J.J. Chinn, An appraisal of swirl atomizer inviscid flow analysis, part 2: inviscid spray cone angle analysis and comparison of inviscid methods with experimental results for discharge coefficient, air core radius, and spray cone angle, Atom. Sprays 19 (2009) 283–308.
[20] A.L. Yarin, Free Liquid Jets and Films: Hydrodynamics and Rheology, Longman Scientific & Technical and Wiley & Sons, Harlow, New York, 1993.

[21] A. Szeri, Tribology: Friction, Lubrication, and Wear, McGraw-Hill, New York, 1980.
[22] T. Azuma, T. Hoshino, The radial flow of a thin liquid film: 4th report, stability of liquid film and wall pressure fluctuation, Bull. JSME 27 (1984) 2763–2770.
[23] T. Azuma, T. Hoshino, The radial flow of a thin liquid film: 1st report, laminar-turbulent transition, Bull. JSME 27 (1984) 2739–2746.
[24] T. Azuma, T. Hoshino, The radial flow of a thin liquid film: 2nd report, liquid film thickness, Bull. JSME 27 (1984) 2747–2754.
[25] T. Azuma, T. Hoshino, The radial flow of a thin liquid film: 3rd report, velocity profile, Bull. JSME 27 (1984) 2755–2762.
[26] J.H. Arakeri, K.P.A. Rao, On radial film flow on a horizontal surface and the circular hydraulic jump, J. Indian Inst. Sci. 76 (1996) 73–91.
[27] G. Park, J. Lee, S. Oh, Y. Yoon, C.H. Sohn, Characteristics of gas-centered swirl coaxial injector with acoustic excitation of gas flow, AIAA J. 55 (2017) 894–901.
[28] J. Doupovec, A.L. Yarin, Nonsymmetrical modified chemical vapor deposition (N-MCVD) process, J. Lightw. Technol. 9 (1991) 695–700.
[29] L.G. Loitsyanskii, Mechanics of Liquids and Gases, Pergamon Press, Oxford, 1966.
[30] H. Schlichting, Boundary Layer Theory, McGraw-Hill, New York, 1979.